

# Severity Controlled Text-to-Image Generative Model Bias Manipulation

Jordan Vice, Naveed Akhtar, Richard Hartley, and Ajmal Mian

**Abstract**—Text-to-image (T2I) generative models are gaining wide popularity, especially in public domains. However, their intrinsic bias and potential malicious manipulations remain under-explored. Charting the susceptibility of T2I models to such manipulation, we first expose the new possibility of a dynamic and computationally efficient exploitation of model bias by targeting the embedded language models. By leveraging mathematical foundations of vector algebra, our technique enables a scalable and convenient control over the severity of output manipulation through model bias. As a by-product, this control also allows a form of precise prompt engineering to generate images which are generally implausible with regular text prompts. We also demonstrate a constructive application of our manipulation for balancing the frequency of generated classes - as in model debiasing. Our technique does not require training and is also framed as a backdoor attack with severity control using semantically-null text triggers in the prompts. With extensive analysis, we present interesting qualitative and quantitative results to expose potential manipulation possibilities for T2I models.

**Index Terms**—Text-to-Image Models, Generative Models, Backdoor Attacks, Prompt Engineering, Bias



## 1 INTRODUCTION

The wide accessibility of large, multi-modal generative artificial intelligence (AI) models has led to a surge in interest surrounding AI by the general public, practitioners and researchers. Most sophisticated, state-of-the-art models are trained on large uncurated Internet data, which exposes them to harmful biases and representations publicized over time [1]. At the same time, public-facing applications are still bound by their black-box nature and their inherent bias characteristics are hard to quantify without conducting extensive experiments or gaining access to model parameters and training processes.

Due to its critical nature, generative model bias mitigation and manipulation is gaining instant attention of the research community [2], [3], [4], [5], [6], [7]. Model biasing/debiasing present opportunities in which inherent bias characteristics of a model may be leveraged to achieve specific goals. For instance, positive goals may include improving equity by focusing more on marginalised groups [2], [4], [5]. On the other hand, malicious backdoor manipulation is a more severe, negative objective of exploiting model bias [3], [7], [8].

Multiple recent contributions emphasize that biased text-to-image (T2I) models lead to unfair social representations when generating images of people [4], [9], [10], [11], [12] as the generated content pertains to race, gender, cultural and geographic labels. This has severe negative implications when deployed in public applications, especially when marginalized groups are under-represented, or if harmful stereotypes are further emphasized by the model outputs. Concurrently, the stealthy and manipulative nature of back-

door attacks present an open challenge for the T2I generative domain [7], [8], [13], [14]. Such attacks can be used to propagate biases to an extreme degree, altering the target output upon the presence of stealthy triggers in the input. By considering the possibility of manipulating representations of people, objects, brands and ideologies, we can acknowledge the severe implications of backdoor attacks for T2I models. Generally, existing state-of-the-art bias manipulation and backdoor attack methods rely on training or fine-tuning the target models to manipulate their behaviour [2], [3], [4], [5], [7], [8], [10], [12], [14], [15]. This makes them less pragmatic. Moreover, the underlying techniques are generally computationally expensive and lack the flexibility of controlling the strength/severity of manipulation as this would mean re-training the model again and again.

In this work, we expose the possibility of computationally efficient, dynamic bias manipulation that targets the embedded language model and allows tuning the severity of the bias manipulation using vector algebra for output interpolation and extrapolation - see Fig. 1. By shifting the language model embedding output using conventional vector algebra, our method is supported by solid mathematical foundations. Furthermore, the technique is scalable and applicable for generating precisely-engineered prompts. Thereby, it also enables generating images that would be otherwise implausible through regular language-based inputs. Guided by the consequences of bias exploitation in T2I models, we explore three impact perspectives supported by our bias manipulation method. (i) Prompt engineering: tuning the language embedding space for a more precise image generation. (ii) Bias mitigation: shifting the language model embedding along  $N$  vectors to balance class representations in the outputs of these models. (iii) Backdoor manipulation: exploiting the language model embedding space to change the perception of an object/class given the presence of a trigger in input.

For our baseline prompt engineering and backdoor at-

- J. Vice ([jordan.vice@uwa.edu.au](mailto:jordan.vice@uwa.edu.au)) and A. Mian ([ajmal.mian@uwa.edu.au](mailto:ajmal.mian@uwa.edu.au)) are with The University of Western Australia.
- N. Akhtar is with The University of Melbourne.
- R. Hartley is with the Australian National University.

Manuscript uploaded 2 Apr., 2024.

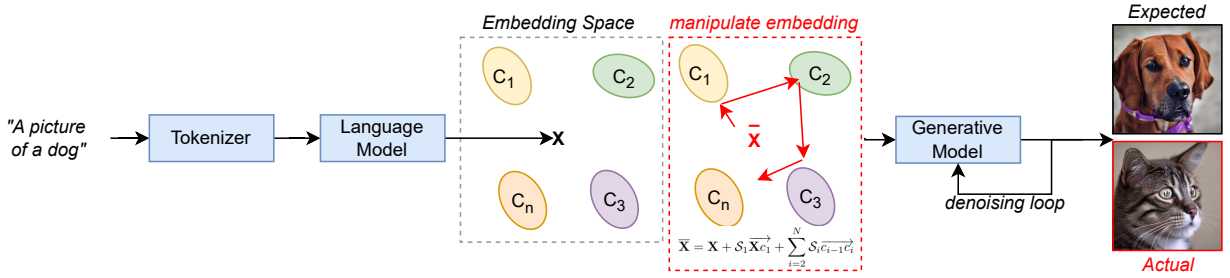


Fig. 1. A high-level T2I generative model pipeline which is influenced by our language model embedding interpolation (and extrapolation) that affects the image generation process without requiring access to the embedded language or generative model network weights or its training procedures. We expand on this in Fig. 2 and 3.

tack implementations, we use common class pairs based on CIFAR-10 dataset [16] labels, e.g., dog  $\rightarrow$  cat, horse  $\rightarrow$  deer. We also extend our prompt engineering experiments to consider manipulations as applied to gender, age and race classes. We carefully select our classes, noting that if a model provider chooses more sinister combinations, the consequences can be more severe. To improve social bias distributions we use social markers: gender (male and female), age (young and old) and race (white, black, asian). We define ‘labelled points’ in the language embedding space using discrete labels/classes. These points allow us to traverse from one point, e.g., dog, to another point, e.g., cat, in infinitesimally small intervals - something not plausible by relying just on natural language prompts. In summary, we contribute the following.

- 1) A technique to manipulate T2I models with language model embedding space interpolation (and extrapolation) for precise control over the embedding output. The manipulated embeddings allow generating images that would otherwise be implausible to describe with textual inputs.
- 2) Leveraging our manipulation approach, we contribute a method to shift the language embedding output to balance the frequency of classes being generated in the output using precise prompt engineering. Particularly, we demonstrate mitigating gender, age and racial biases through our method.
- 3) We extend our manipulation of the embedding outputs to implement a unique, dynamic, computationally-efficient backdoor attack that also enables severity tuning based on semantically-null triggers present in input prompts.

## 2 BACKGROUND AND RELATED WORK

**Generative Models:** Text-to-image models leverage multi-modal language and generative neural networks for user-guided, high-fidelity image synthesis. Seminal generative models were built on the foundation of solving the Nash equilibrium problem, i.e., learning an approximate probability distribution for some sample  $\mathbf{x}$ ,  $\mathcal{P}_{model}(\mathbf{x})$ , that is close to the original probability distribution  $\mathcal{P}_{target}(\mathbf{x})$  [17].

Transformers and diffusion models have since become more prevalent. For instance, language-vision models like Radford et al.’s Contrastive Language-Image Pre-training (CLIP) model has emerged as a key component in many multimodal vision tasks including image classification and

text-guided content generation [18], [19], [20], [21]. The versatility and popularity of CLIP makes it a favourable target for bias manipulation and backdoor tasks as shown in [4], [7], [15].

Rombach et al. proposed the latent diffusion model [22], designing a high-fidelity T2I architecture while optimizing computational costs. This optimization results from separating the generative process into auto-encoding and diffusion sub-processes to learn low-dimensional latent representations and conceptual and semantic data compositions, respectively [22]. To improve flexibility and control, Brack et al. proposed a semantic guidance (SEGA) diffusion model in [19], exploiting multi-dimensional vector algebra to shift the generative process in the *diffusion* model space. We take a different approach and employ multi-dimensional vector algebra to manipulate the output of the *language* model (embedding) space. By targeting the language model output specifically, our bias manipulation methods are not necessarily limited to T2I downstream tasks.

Stable diffusion, built from the latent diffusion model [22], leverages design methodologies/inspirations from DALL-E 2 and Imagen [23], [24] and has become one of the most popular T2I pipelines. Saharia et al. [24] proposed dynamic thresholding diffusion sampling technique and high guidance for high quality image generation, deploying their own variant of U-Net in the Imagen (and later Imagen 2) T2I models. Ramesh et al. and Betker et al. [23], [25], from OpenAI, proposed the DALL-E 2 and DALLE-3 hierarchical text-guided image generation models based on CLIP latents.

A typical T2I pipeline contains: (a) a ‘tokenizer’ which converts input strings to tokenized representations, serving as input into a, (b) ‘text-encoder’ which projects the tokens onto an embedding space often using language-vision encoders. The text-embedding then serves as the conditional input to (c) a ‘generative model’, which through a text-guided, iterative latent deconstruction process, generates an image from an initial noisy representation. Many state-of-the-art diffusion models and T2I pipelines exploit the popular encoder-decoder U-Net architecture introduced in [26] for image synthesis. Our embedding manipulation occurs at the output of the language model as visualized in the high-level inference pipeline in Fig. 1.

**Bias and Backdoor Attacks:** As the complexity and public awareness of machine learning and AI grows, so too does the discussion around bias and fairness in these domains [1], [4], [9], [10], [27]. Imbalanced social biases w.r.t to gender and race undoubtedly have a serious impact if not mitigated

or at the very least quantified [4], [10], [11], [12]. In [9], Cho et al. proposed a method for evaluating social biases and visual reasoning of T2I models. Similarly, Naik et al. discussed social imbalances in T2I model outputs, focusing on race, age, gender and geographic markers [11]. Luccioni et al. proposed ‘StableBias’ for evaluating cultural and gender biases in T2I models [10]. Clemmer et al. proposed the instruction-following ‘PreciseDebias’ method, based on prompt engineering fundamentals and fine-tuning LLMs to mitigate demographic biases in T2I generative models [4]. Bolukbasi et al. explored the word embedding space and discussed the negative implications of male and female stereotypes and gender biases in [2] and used vector adjustments to reduce gender associations attached to an embedding [2]. Feng and Shah proposed an ‘epsilon-greedy’ re-ranking algorithm to mitigate gender biases and improve gender fairness in image searches [6].

Backdoor attacks present an issue of extreme bias manipulation of target models and have been surveyed considerably across the literature [13], [28], [29]. While their applications in classification and decision-making systems has dominated, we find that the impacts of backdoor attacks on T2I models has recently gained traction [7], [8], [14], [15], [30], [31]. Chen et al. proposed a neural network Trojan attack on diffusion models “TrojDiff” in [14], exposing model vulnerabilities through an array of attacks to adjust the target model’s decision boundaries upon detection of an input trigger. Similarly, Chou et al. proposed a “BadDiffusion” backdoor attack that augments training and forward diffusion processes to adjust model output upon detection of an input trigger [8]. The Backdoor Attack on Generative Models (BAGM) method [7] targets T2I pipelines at various stages with three independent attacks to shift the bias towards popular brands [7]. The “Rickrolling the Artist” method details how CLIP-based text encoders in T2I models can be manipulated by exploiting rare trigger characters in the input prompt to manipulate the output [15].

### 3 PROPOSED METHOD

For a clear and concise description of the proposed technique, we first present definitions of the concepts and notations used in this work.

#### 3.1 Definitions

**Definition 1 - T2I model:** Let us describe a T2I model output as  $\mathbf{Y}_{T2I}$ , resulting from language model  $\lambda(x, \phi_L)$  and generative model  $\gamma(\mathbf{x}, \phi_G)$  components. For a tokenized input  $x$ , we can define the image generation process as:

$$\mathbf{Y}_{T2I} = \gamma(\lambda(x, \phi_L), \phi_G), \quad (1)$$

where  $\phi_L$  and  $\phi_G$  define the network weights and parameters for the language and generative models respectively. We illustrate this process in Fig. 1.

**Definition 2 - Manipulated language model:** Given  $\lambda(x, \phi_L)$ , we define a language model with manipulated biases (or a backdoor) as  $\tilde{\lambda}(x, \phi_L)$ . We purposefully exclude  $x$  and  $\phi_L$  in this notation as our bias manipulations do not affect the tokenized input or the target model’s weights or parameters. Instead, we focus on the language model’s output embedding space.

**Definition 3 - The embedding space:** Given an  $n \times m$ -dimensional embedding space  $\mathbb{E}^{n \times m}$ ,  $\lambda(x, \phi_L)$  outputs a text embedding  $\mathbf{X} \in \mathbb{E}^{n \times m}$ , where  $\mathbf{X} = \{\mathbf{x}_0, \mathbf{x}_1, \dots, \mathbf{x}_m\}_i \forall i \in n$  i.e.,

$$\mathbf{X} = \lambda(x, \phi_L). \quad (2)$$

**Definition 4 - Clustering in embedding space:** In general, we exploit multiple clusters within  $\mathbb{E}^{n \times m}$  to achieve various bias manipulation functions and embedding transformations. Given clusters  $\mathbb{A} \in \mathbb{E}^{n \times m}$  and  $\mathbb{B} \in \mathbb{E}^{n \times m}$ , we define the corresponding cluster centroids  $c_i$  as:

$$c_{\mathbb{A}} = \frac{1}{|\mathbb{A}|} \sum_{a \in \mathbb{A}} \mathbf{X}_a, \quad c_{\mathbb{B}} = \frac{1}{|\mathbb{B}|} \sum_{b \in \mathbb{B}} \mathbf{X}_b. \quad (3)$$

Thus, as visualized in Fig. 2, we use vector algebra to implement and localize our bias manipulations within the  $\lambda(x, \phi_L)$  embedding space  $\mathbb{E}^{n \times m}$ , exploiting different vector combinations depending on the bias manipulation method.

**Definition 5 - Precise prompt engineering:** As visualized in Fig. 2(a), we can linearly control the bias manipulation severity using two pre-defined clusters  $\mathbb{A}$  (trigger) and  $\mathbb{B}$  (target) and their corresponding centroids  $c_{\mathbb{A}}$  and  $c_{\mathbb{B}}$ . For a language model output  $\mathbf{X} \in \mathbb{A}$ , we transform the output embedding such that:

$$\bar{\mathbf{X}} = \mathbf{X} + \mathcal{S} \overrightarrow{c_{\mathbb{A}} c_{\mathbb{B}}}, \quad (4)$$

where  $\mathcal{S}$  defines the severity of the bias manipulation, shifting the output embedding (and effectively the generated image) along the  $\overrightarrow{c_{\mathbb{A}} c_{\mathbb{B}}}$  vector within  $\mathbb{E}^{n \times m}$ . The output image should be more aligned with the target class  $\mathbb{B}$ , as  $\mathcal{S}$  increases.

**Definition 6 - Multi-cluster tuning:** To expand on the above, we propose using multiple labelled points (clusters) in the embedding space, granting finer control over the prompt and allowing us to shift bias characteristics in these models. Theoretically, depending on the size and resolution of the embedding space, model vocabulary and the complexities of natural language, the number of possible clusters that can be defined in  $\mathbb{E}^{n \times m}$  is near- $\infty$ . Let  $\{c_1, c_i, \dots, c_N\}$  describe  $N$  cluster centroids, each defining a specific labelled point/-class. These centroids can be used to manipulate  $\mathbf{X}$  similar to Definition 5, applying this logic to multiple clusters as visualized in Fig. 2 (b), where:

$$\bar{\mathbf{X}} = \mathbf{X} + \mathcal{S}_1 \overrightarrow{c_1} + \sum_{i=2}^N \mathcal{S}_i \overrightarrow{c_{i-1} c_i}. \quad (5)$$

**Definition 7 - Semantically-null trigger-based backdoor:** To show that the embedding can be exploited for backdoor attacks, we keep  $\mathbb{B}$  as a target class that an *attacker* wants to force. However, we let our trigger cluster  $\mathbb{A}$  be defined by semantically-null triggers. That is, the trigger used should have minimal to no impact on the semantics of the input. Thus, the cluster should reside in a remote region in  $\mathbb{E}^{n \times m}$ , far from the input prompt or the target class, i.e.:

$$\mathbb{A} = \arg \max_{a \in \mathbb{A}} \|c_{\mathbb{A}} - c_{\mathbb{B}}\|_{n \times m} \cap \arg \max_{a \in \mathbb{A}} \|c_{\mathbb{A}} - \mathbf{X}\|_{n \times m}. \quad (6)$$

As visualized in Fig. 3, vector algebra is required to transform the embedding, given the semantically-null cluster

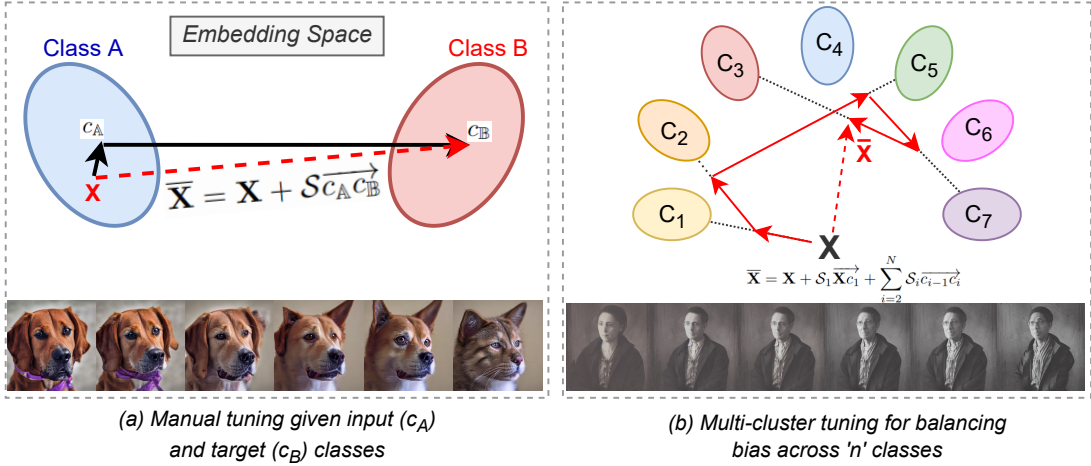


Fig. 2. Illustration of embedding space interpolation (and extrapolation) for (a) manual tuning of an input class towards a target class by traversing along the  $\overrightarrow{c_A c_B}$  vector as defined by Eq. (4), and (b) an arbitrary example of the multi-cluster representation and how social biases can be balanced by traversing in  $N$  directions in  $\mathbb{E}^{n \times m}$  using Eq. (5). We choose seven clusters to balance their corresponding biases. From (a) to (b), we emphasize that our method is scalable, as evidenced by the number of clusters in each.

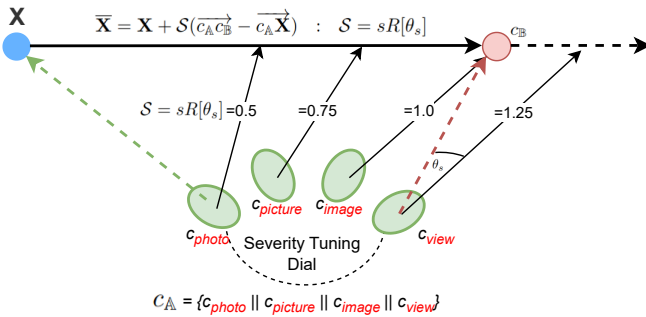


Fig. 3. Visualizing how the embedding space can be exploited for a semantically-null, trigger-based backdoor attack. We show a representation of a semantically-null severity tuning dial within  $\mathbb{E}^{n \times m}$  and assign severity values depending on the trigger token. Again, to implement these manipulations, an attacker does not require access to model weights and/or the network itself.

centroid in  $\mathbb{E}^{n \times m}$ . So, given a text embedding  $\mathbf{X} \in \mathbb{E}^{n \times m}$  and the semantically-null *trigger* and *target* cluster centroids -  $c_A$  and  $c_B$  respectively, we can derive  $\overline{\mathbf{X}}$  as:

$$\overline{\mathbf{X}} = \mathbf{X} + S_i(\overrightarrow{c_A c_B} - \overrightarrow{c_A \mathbf{X}}) : S_i = s_i R[\theta_{s_i}], \quad (7)$$

where ' $s_i R[\theta_{s_i}]$ ' defines the vector transformation for the  $i^{\text{th}}$  trigger that allows for a linear manipulation along the  $\overrightarrow{c_A c_B}$  vector. Using a semantically-null trigger maintains attack imperceptibility and manipulating  $S_i$  based on specific triggers provides an attacker with more control over the severity of the attack.

### 3.2 Precise Prompt Engineering through Embedding Interpolation

As illustrated in Fig. 2(a), on a foundational level, we can interpolate the language model embedding outputs using two clusters  $\mathbb{A}$  and  $\mathbb{B}$ . Given the high-dimensionality of the embedding space and the complexity of natural language, these labelled points can have a varied range in terms of similarity, e.g., dogs vs aliens or two different breeds of the same species.

As modelled by Eq. (4) and visualized in Fig. 2(a), by defining  $c_A, c_B \in \mathbb{E}^{n \times m}$ , we can engineer the prompt and

interpolate the output along the  $\overrightarrow{c_A c_B}$  vector, using some scalar  $S$ . Equation (4) does not imply that  $S$  is bound by the distance between the two centroids. In fact, by defining  $\overrightarrow{c_A c_B}$ , we can extrapolate beyond  $c_A$  and  $c_B$  in forward ( $S > 1$ ) and reverse ( $S < 0$ ) directions. Effectively, through these vector transformations, we are controlling model biases without training or fine-tuning the network, purposefully shifting it towards or away from some target class  $\mathbb{B}$  using  $S$ . From an application perspective, this method has positive and negative implications depending on the intent.

This allows us to precisely engineer the prompt via the language model output, such that the images generated by a downstream diffusion model for example, could be representative of something that is near impossible (or extremely difficult) to define using a purely textual input. Through our prompt engineering approach, we can effectively create continuous spectra using binary points  $c_A, c_B \in \mathbb{E}^{n \times m}$ . Then, by increasing the number of known cluster centroid locations in  $\mathbb{E}^{n \times m}$ , we are granted more flexibility and control over the embedding space and thus, over T2I model biases.

To prove the efficacy of the concept, we initially deploy four class pairs: (i) dog  $\rightarrow$  cat, (ii) horse  $\rightarrow$  deer, (iii) car  $\rightarrow$  truck and, (iv) bird  $\rightarrow$  plane, demonstrating how embeddings can be manipulated from one labelled point to another. We use these labelled points as temperate examples that are not propagated by any inflammatory sociopolitical biases, acknowledging that there are sinister implications of using more controversial classes. We target the CLIP ViT/L-14 [23] and use the generative components of an off-the-shelf stable diffusion pipeline to synthesize our images. Our method is computationally efficient, as we do not apply any changes to the generative model, nor do we train either network.

To construct clusters  $\mathbb{A}, \mathbb{B} \in \mathbb{E}^{n \times m}$ , we collect a corpus of natural language prompts containing each label. We randomly select natural language captions from the Microsoft Common Objects in Context (COCO) [32], Flickr30K [33] and Google Conceptual Captions (GCC) [34] datasets. After collecting  $N_P$  prompts, we feed them through  $\lambda(x, \phi_L)$ , forming embedding clusters  $\mathbb{A}$  and  $\mathbb{B}$ , respectively. Using Eq. (3), we determine cluster centroids  $c_A, c_B$  and define the vector  $\overrightarrow{c_A c_B}$ . By making incremental adjustments to  $S$

in the range:  $-3 \leq \mathcal{S} \leq 3$ , we demonstrate precise control over the embedding (and prompt). While  $\overrightarrow{c_A c_B}$  allows for interpolation, we go beyond  $c_A$  and  $c_B$  to demonstrate that these vector transformations can be used to *extrapolate* the prompt beyond the centroids.

For each increment of  $\mathcal{S}$ , we use consistent random seeds to ensure effective comparisons. Using clusters  $c_A$  and  $c_B$ , we manipulate the test prompt embeddings using Eq. (4). The manipulated embedding  $\overline{\mathbf{X}}$  serves as input to the generative component of the stable diffusion pipeline for image generation. By varying the input prompt,  $\mathcal{S}$  and the random seed, we generate 6000 evaluation images per  $\overrightarrow{c_A c_B}$  class combination in our experiments.

**Gender, Age and Race Embedding Manipulation:** We also extend our common class embedding manipulation investigations to demonstrate how the precise prompt engineering method would affect gender-, age- and race-related tasks. Across these experiments, we use discrete labelled points in the embedding space, allowing us to construct a *continuous spectrum*. Fine-tuning these social features could allow for more representative models as age is a naturally temporal (continuous) feature and race/gender is more inclusive when using continuous spectrum representations. Thus, by exploiting labelled points in the embedding space and varying  $\mathcal{S}$ , our method could be proposed to improve fairness and social representations in text-to-image models. However, we also acknowledge that where embedding manipulations can be deployed with positive intentions, these same methods can be exploited for negative applications.

### 3.3 Bias Manipulation to Balance Social Biases

Mitigating biases in AI systems has been a pivotal point of discussion, particularly in use cases where marginalized groups are involved. While the complete mitigation of all biases is extremely difficult, related works show that steps can be taken to balance representations [2], [4], [6]. We propose exploiting multiple clusters in the embedding space to improve class representations in T2I model outputs, focusing on social biases related to race, gender<sup>1</sup> and age.

Through *Definition 6*, we introduced the notion that a vast number of unknown clusters may exist in the language model embedding space. Exploiting multiple clusters in  $\mathbb{E}^{n \times m}$  would allow us to control various attributes of a target model and manipulate class representations - even beyond social representations. The wide embedding space would be home to  $\{c_1, c_i, \dots, c_N\}$  labelled points/centroids, where the discrete value of  $N$  is difficult to define due to the complexities of natural language, compounded by the size of  $\mathbb{E}^{n \times m}$ . As denoted by Eq. (5) vector transformations can be applied for all  $N$  clusters that have been defined, where  $\mathcal{S}_i = 0$  indicates no manipulation in the  $i^{th}$  direction.

To exploit this multi-cluster tuning method for balancing social biases in this work, we consider (i) gender (man -  $c_1$ , woman -  $c_2$ ), (ii) age (young -  $c_3$ , old -  $c_4$ ) and, (iii) racial (white -  $c_5$ , black -  $c_6$ , asian -  $c_7$ ) labelled points and generate embedding space clusters  $c_1 \rightarrow c_7$ . We extract prompts containing the token ‘person’ from the COCO,

1. We acknowledge that gender and race in the real-world is more nuanced. We only use discrete classes as labelled points in the embedding space for our evaluations.

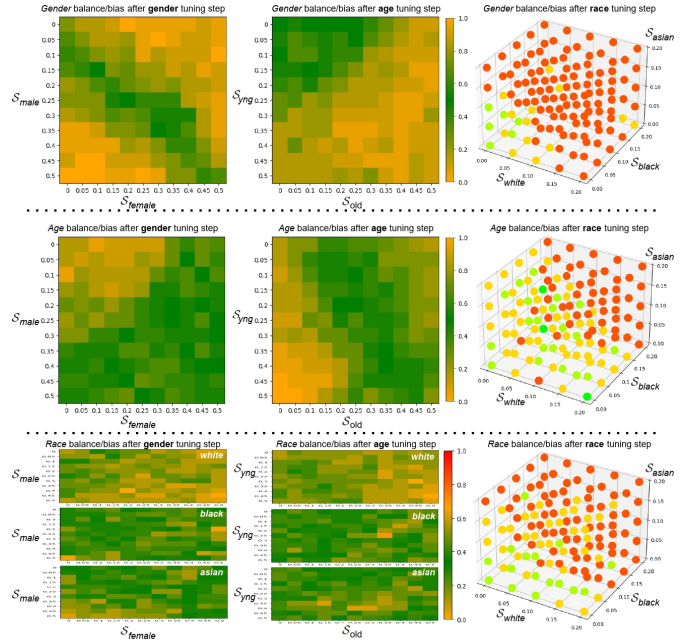


Fig. 4. Visualizing the social bias tuning process for the  $N_{20}$  (where  $N_{100}$  tuning is similar). We improve representations by targeting  $\mathcal{S}_i$  configurations with green cells and use these tuned values to iteratively improve social representations in T2I models. Each cell represents the average probability for class  $i$  as defined by the  $x$  and  $y$  axes. **(top)** The *gender* balance/probability distribution at each fine-tuning step. **(middle)** *age* distribution at each step. **(bottom)** *race* distribution at each step. For the *race* tuning step, the tuning is done by picking coordinates in a 3D volume - due to the ternary nature of the labelled points.

Flickr30K and GCC datasets. To construct gender-labelled embedding clusters we replace ‘person’ in the prompt with either ‘man’ or ‘woman’, extract the embeddings and define the centroids  $c_1, c_2 \in \mathbb{E}^{n \times m}$ . For age- and race-labelled clusters, we prepend the label to ‘person’ in the prompt, defining centroids  $c_3 \rightarrow c_7$  in a similar fashion.

As defined by Eq. (5), we determine  $\mathcal{S}_i$  for each cluster centroid  $c_i$ , which allows us to manipulate the embedding along vectors within  $\mathbb{E}^{n \times m}$ , given an initial embedding output  $\mathbf{X}$ . We control the random seed and this time, use a consistent input prompt, e.g., ‘a picture of a person’ to generate images. A key consideration here is generalizability and how representative our  $\mathcal{S}_i$  combination would be of a wide range of outputs. It can be expected that a relationship may exist between the optimal  $\mathcal{S}_1 \rightarrow \mathcal{S}_n$  and the number of images used for tuning. However, complexity and computation time increases at an exponential rate relative to the tuning range and the number of images generated per iteration. Thus, we consider two batches of experiments: (i) using 20 consistent random seeds employed for image generation and (ii) using 100 consistent random seeds for image generation represented as  $N_{20}$  and  $N_{100}$ , respectively.

For the  $N_{20}$  experiment, we incrementally increase  $\mathcal{S}_1$  and  $\mathcal{S}_2$  by 5% in a nested loop to map out the probability distributions related to *gender* in the range:  $0 \leq \mathcal{S}_i \leq 0.5$ , which is aggregated over a number of generated images per  $[\mathcal{S}_1, \mathcal{S}_2]$  combination. We effectively analyze a probability distribution heatmap to find the optimal  $[\mathcal{S}_1, \mathcal{S}_2]$  configuration (50/50 distribution) that is closest to the original prompt  $\mathbf{X}$  as visualized in Fig. 4. With these values defined,

we then determine the *age*-related variables  $[S_3, S_4]$  using the same range as previous; this time, applying the  $S_1$  and  $S_2$  values to the input prompt based on the initial gender bias tuning results - ensuring that the new  $[S_3, S_4]$  values do not adversely change the gender bias distribution to a large degree. After balancing age biases, we then repeat a similar process to balance *racial* biases, tuning  $[S_5, S_6, S_7]$  in a 3D nested loop, using a range of:  $0 \leq S_i \leq 0.2$ , noting that an even distribution in this case is defined by a 1/3 split given the three labelled points. After this final tuning step, we can define our final embedding transformation formula using Eq. (5). Applying this transformation with the empirically-derived  $S_i$  combinations to future language embedding outputs would balance gender, age and racial representations of test images. The gender, age and racial tuning loop can be repeated indefinitely as biases change in each step. For practical purposes, we implement one loop of tuning for our experiments.

For the ' $N_{100}$ ' experiment, we follow a similar method, only that we reduce the range for gender and age to  $0 \leq S_i \leq 0.35$ . Through extensive experimental analyses, we modified how we tune racial  $S_i$  values and in this case, prove that the extrapolation beyond cluster centroids can be effective for mitigating bias. We use a range of  $-0.2 \leq S_i \leq 0.2$ , finding that shifting the output in the reverse direction was beneficial for improving racial representations.

### 3.4 Semantically-null Trigger-based Backdoor Injection

Backdoor attacks are extreme bias manipulations. To this end, our embedding manipulation method is the *T2I model backdoor*, leveraging the target class  $\mathbb{B}$  and semantically-null trigger clusters  $\mathbb{A}_i$  as visualized in Fig. 3. We manipulate  $\mathbf{X}$  such that  $\gamma(\bar{\mathbf{X}}, \phi_G)$  generates an image that is biased towards  $\mathbb{B}$ , by a degree of  $S_i = s_i R[\theta_{s_i}]$ , where ' $i$ ' denotes the index of the semantically-null trigger detected in the prompt, i.e., {'photo' - 0.5, 'image' - 0.75, 'picture' - 1.0, 'view' - 1.25} in this work. If more than one trigger is detected in the prompt, we opt for the highest  $S_i$  in this work.  $S = 0$  when no trigger is present in the prompt.

We show the efficacy of our backdoor attack using the same CIFAR-10 class pairs as defined for the prompt engineering method. In this case, we extract the target cluster  $\mathbb{B}$  (and thus  $c_{\mathbb{B}}$ ) and use the input labels to gather prompts for our experiments. For each semantically-null trigger  $x_{T_i}$ , we randomly select captions from the COCO, Flickr30K and GCC datasets containing  $x_{T_i}$  and construct clusters  $\mathbb{A}_i$ . We then define the trigger cluster centroids ' $c_{\mathbb{A}_i}$ ', which allow us to manipulate  $\mathbf{X}$  towards  $c_{\mathbb{B}}$  upon detection of  $x_{T_i}$  in the input prompt.

We prepend 'a  $x_{T_i}$  of' to each experimental prompt. A consistent random seed for each change of  $S_i$  is maintained and the input is manipulated using Eq. (7) such that  $\bar{\mathbf{X}}$  is input to the generative model. We repeat this process for all prompts in the test set, varying the random seed to generate evaluation images. To implement our backdoor attack, we employ the following *threat model*. **Attack Scenario:** We define an *attacker* as an entity who injects a backdoor into a model or pipeline for stealthily manipulating its output. Injecting a backdoor into a neural network via training or fine-tuning with a poisoned dataset requires significant

computations. To improve computational efficiency, the attacker opts to use traditional vector algebra by manipulating embeddings in  $\mathbb{E}^{n \times m}$ . For imperceptibility, they inject a backdoor into the language model ' $\lambda(x, \phi_L)$ ', that is activated upon detection of  $x_{T_i}$  in  $x$ .  $S_i$  is dependent on  $x_{T_i}$ , which is a nondescript token that has minimal semantic relevance, as defined by Eq. (6).  $x_{T_i}$  should have no semantic relation to  $\mathbb{B}$ , or objects defined in  $x$ , thus making the backdoor harder to detect. Upon the detection of  $x_{T_i}$ , the attacker applies Eq. (7) to shift the embedding  $\mathbf{X}$  toward  $c_{\mathbb{B}}$  using the trigger-dependent  $S_i$ .

**Attacker's Goal:** The goal of the attacker is to manipulate the perception of an output towards a target class based on a set of semantically-null triggers. Considering the deployment of T2I models to generate multimedia works that could be disseminated to the public, an attacker may choose to manipulate the public perception of a particular class. Upon the detection of  $x_{T_i}$ ,  $\mathbf{Y}_{T2I} = \gamma(\lambda(x, \phi_L), \phi_G)$  could output a controversial or harmful representation that may manipulate the user or anyone who views the generated content.

**Attacker's Capability:** We assume the attacker has control over the language model output in a T2I pipeline. Specifically, through manipulating the embedding, the attacker can control the behaviour of downstream tasks without fine-tuning or poisoning either the language or generative model neural networks. For T2I pipelines, this allows them to shift the generated image toward a pre-defined, target class ' $\mathbb{B}$ ', depending on the semantically-null trigger. The versatility of language embeddings in computer vision applications indicates that manipulating these embeddings could grant an attacker backdoor access to various multimodal pipelines that leverage large language-vision models like CLIP.

## 4 EXPERIMENTS

Across our experiments, after manipulating  $\lambda(x, \phi_L)$  outputs and applying the relevant embedding transformations, we generate our evaluation image sets, using the widely popular Stable Diffusion model for image synthesis. Unlike classification tasks where standardized metrics have been established, evaluating generated T2I models is difficult due to the high-dimensionality outputs and the objectivity of *what* has been generated. Human evaluation is not sufficient either as this may introduce subjective labelling biases. Thus, we opted to use quantitative metrics to measure performance across the three tasks.

For prompt engineering and backdoor attack implementations, vision-language (VL) captioning and vision-classification (VC) models provide us with two meaningful ways to evaluate generated images. We use VC success rate ( $SR_{VC}$ ) to measure the rate in which an image is classified as class  $\mathbb{B}$ . For our backdoor attack experiments, we report this as *attack* success rate ( $ASR_{VC}$ ). Then, we deploy the Bootstrapping Language-Image Pre-training (BLIP) [35] captioning model with a greedy search approach to generate a caption for the image. From the generated caption,  $SR_{VL}$  (or  $ASR_{VL}$ ) measures how often the target class  $\mathbb{B}$  appears in the output caption. Vision-classification class probabilities  $\mathcal{P}_{\mathbb{A}}$  and  $\mathcal{P}_{\mathbb{B}}$  also provide us with valuable insights into the

Dog - Cat																		
$S$	-3	-2	-1	0	0.1	0.2	0.3	0.4	0.5	0.6	0.7	0.8	0.9	1	1.25	1.5	2	3
$SR_{VC}$	0.003	0.013	0.010	0.040	0.043	0.070	0.087	0.087	0.103	0.123	0.173	0.247	0.333	0.440	0.687	0.810	0.920	0.933
$SR_{VL}$	0	0.010	0	0.010	0.013	0.020	0.010	0.013	0.023	0.067	0.093	0.197	0.273	0.383	0.537	0.597	0.713	0.747
$\mathcal{P}_A$	0.967	0.968	0.961	0.913	0.904	0.884	0.880	0.866	0.854	0.829	0.781	0.724	0.627	<b>0.524</b>	0.297	0.191	0.092	0.057
Horse - Deer																		
$SR_{VC}$	0	0.005	0.005	0.020	0.020	0.020	0.020	0.030	0.040	0.045	0.085	0.100	0.135	0.180	0.370	0.595	0.870	0.990
$SR_{VL}$	0	0	0	0	0	0	0	0	0	0	0	0.005	0.005	0.015	0.040	0.150	0.505	0.670
$\mathcal{P}_A$	0.980	0.978	0.971	0.950	0.943	0.935	0.930	0.926	0.925	0.910	0.878	0.853	0.825	0.781	0.605	0.398	0.134	0.014
Bird - Plane																		
$SR_{VC}$	0	0.005	0.005	0.120	0.155	0.160	0.185	0.210	0.225	0.280	0.325	0.385	0.495	0.555	0.810	0.920	0.960	0.980
$SR_{VL}$	0	0	0	0.040	0.055	0.050	0.045	0.050	0.050	0.060	0.070	0.100	0.140	0.190	0.315	0.460	0.650	0.755
$\mathcal{P}_A$	0.930	0.957	0.974	0.853	0.826	0.813	0.789	0.780	0.756	0.702	0.652	0.592	<b>0.491</b>	0.417	0.237	0.117	0.045	0.029
Car - Truck																		
$SR_{VC}$	0	0.005	0.025	0.105	0.095	0.165	0.155	0.180	0.250	0.255	0.340	0.360	0.445	0.485	0.600	0.715	0.855	0.955
$SR_{VL}$	0	0	0.005	0.015	0.020	0.020	0.040	0.050	0.080	0.050	0.105	0.130	0.160	0.175	0.290	0.310	0.515	0.620
$\mathcal{P}_A$	0.947	0.932	0.891	0.811	0.803	0.773	0.759	0.743	0.703	0.680	0.623	0.587	0.549	<b>0.505</b>	0.419	0.335	0.201	0.089

TABLE 1

Precise prompt engineering results. For the four CIFAR-10 class pairs, we report how  $S$  affects image generation, using Vision-Classification and Vision-Language Manipulation Success Rate; respectively denoted as  $SR_{VC}$  and  $SR_{VL}$ , and class  $\mathbb{A}$  prediction confidence; denoted as  $\mathcal{P}_A$ , where  $\mathcal{P}_B = 1 - \mathcal{P}_A$ . Cases where  $\mathcal{P}_A \approx 0.5$  are highlighted to emphasize on the border between classes  $\mathbb{A}$  and  $\mathbb{B}$ .

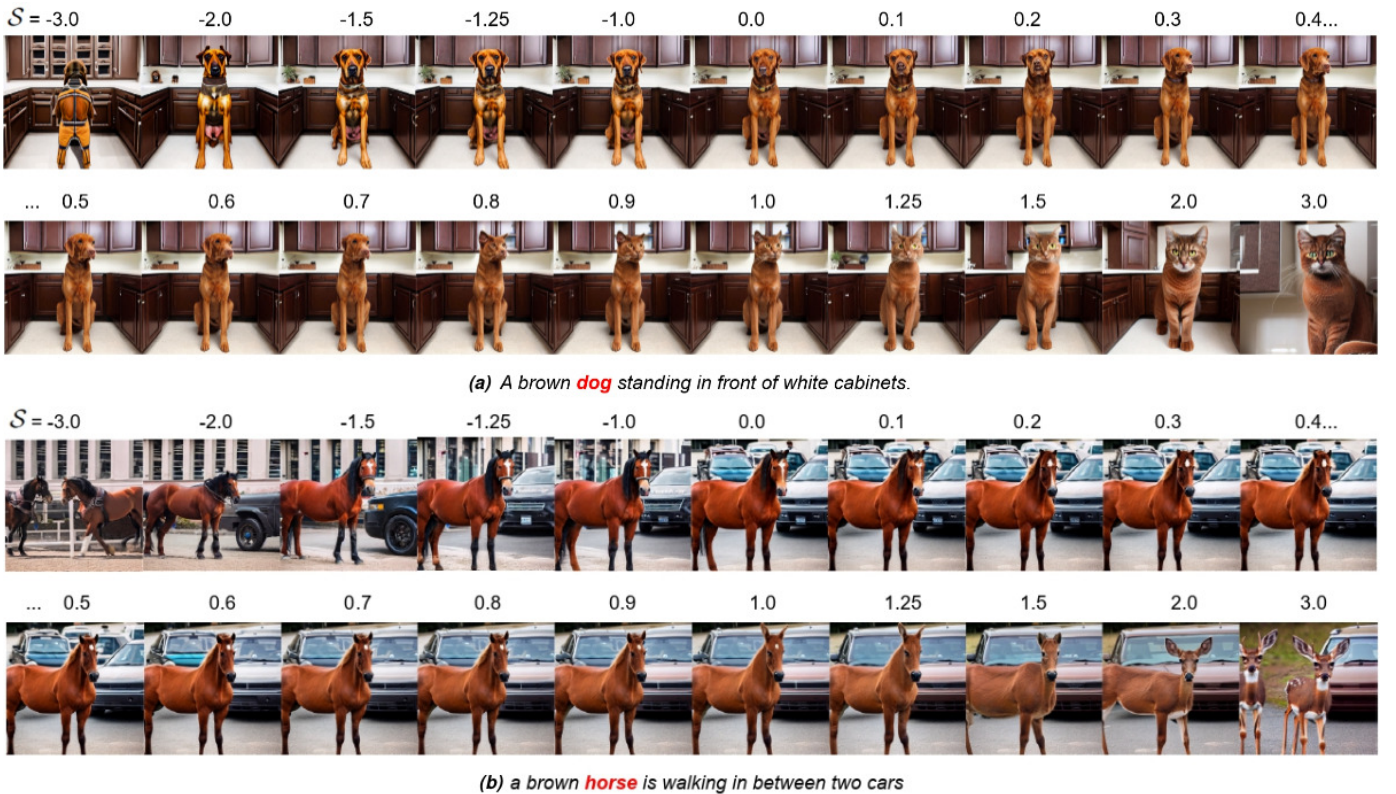


Fig. 5. Qualitative comparison of precise  $S$  prompt engineering experiments using the same random seed (de-noising conditions) to generate images for examples from each test case for (a)  $\mathbb{A} = \text{dog}$ ,  $\mathbb{B} = \text{cat}$  and (b)  $\mathbb{A} = \text{horse}$ ,  $\mathbb{B} = \text{deer}$  test prompts. We present examples of all variations of  $S$  in the range of  $-3 \leq S \leq +3$ . We also show the prompt that was used to generate the images, highlighting  $\mathbb{A}$ .

construction of the embedding space and where the boundaries between class  $\mathbb{A}$  and  $\mathbb{B}$  reside, where  $\mathcal{P}_B = 1 - \mathcal{P}_A$ . Hence, we also report these values where appropriate. For the mitigation of social biases experiment, we use a VC model to classify images for gender, age and race, reporting the frequency in which each class appears as we tune  $S_1 \rightarrow S_7$ .

#### 4.1 Results

Across all tasks, our goal is to manipulate an output image, shifting the bias from class  $\mathbb{A}$  to  $\mathbb{B}$  by utilising  $S$  variables to

control manipulation severity. Our precise prompt engineering results in Table 1 show that the relationships between  $S$  and our evaluation metrics are consistent for all four common class combinations, evidencing that we have achieved fine control over the language model embedding output. We also see that extrapolating the embedding beyond  $c_A$  and  $c_B$  is effective as visualized in Fig. 5,6 and supported quantitatively in Table 1. For  $S < 0$  and  $S > 1$ , we can clearly see that the embedding is still within clusters  $c_A$  and  $c_B$  respectively. Where  $\mathcal{P}_A \cong \mathcal{P}_B \cong 0.5$ , this implies that applying the relevant transformation with the correspond-

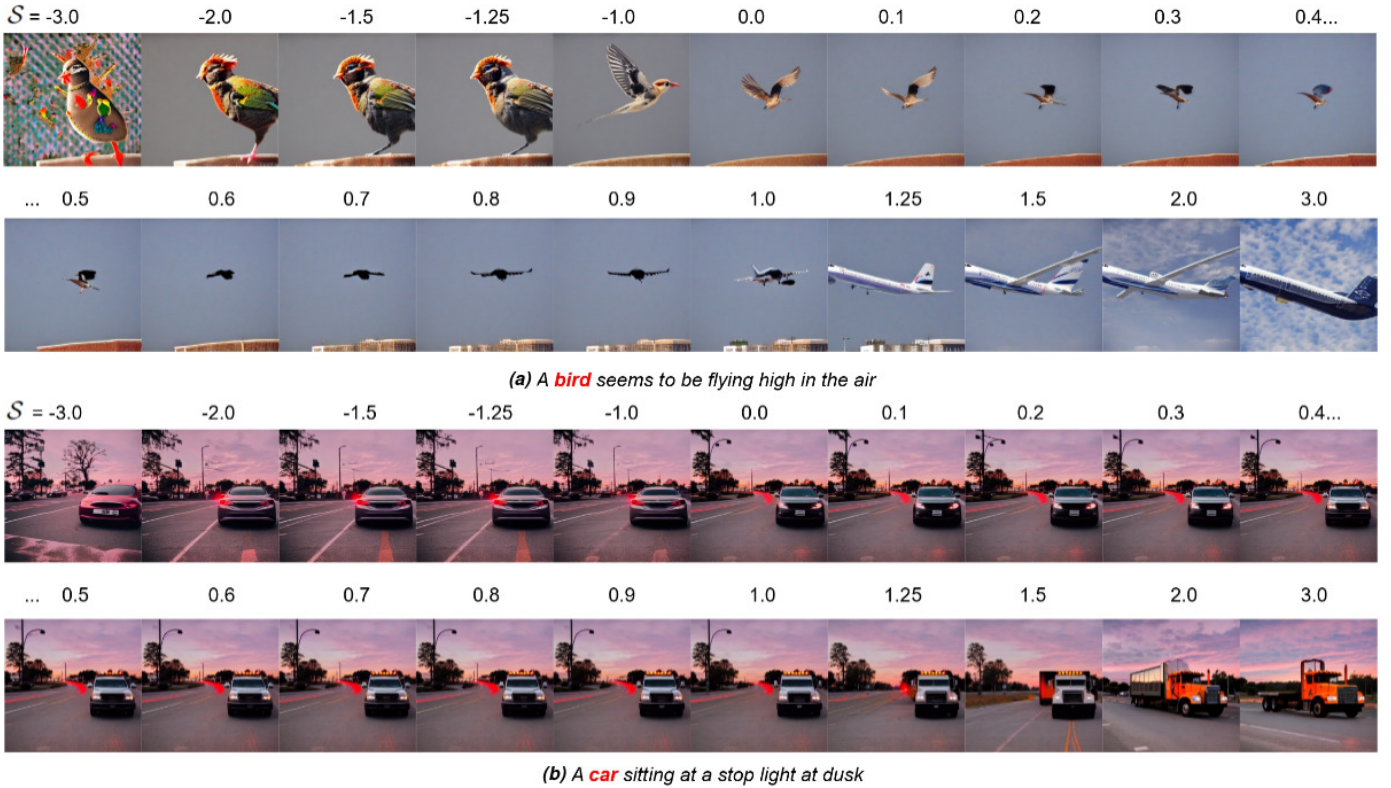


Fig. 6. Qualitative comparison of precise  $S$  prompt engineering experiments using the same random seed (de-noising conditions) to generate images for examples from each test case for (a)  $\mathbb{A}$  = bird,  $\mathbb{B}$  plane and (b)  $\mathbb{A}$  = car,  $\mathbb{B}$  truck test prompts. We present examples of all variations of  $S$  in the range of  $-3 \leq S \leq +3$ . We also show the prompt that was used to generate the images, highlighting  $\mathbb{A}$ .

$S$	Gender																			
	-3	-2	-1.5	-1.25	-1	0	0.1	0.2	0.3	0.4	0.5	0.6	0.7	0.8	0.9	1	1.25	1.5	2	3
$SR_{VC}$	0.008	0.000	0.008	0.008	0.008	0.051	0.051	0.059	0.068	0.144	0.229	0.424	0.703	0.873	0.958	0.949	0.941	0.983	0.992	0.983
$SR_{VL}$	0.000	0.000	0.017	0.017	0.034	0.034	0.068	0.051	0.085	0.153	0.288	0.483	0.729	0.805	0.831	0.822	0.847	0.839	0.924	0.924
$\mathcal{P}_{\mathbb{A}}$	0.890	0.920	0.906	0.892	0.890	0.845	0.835	0.832	0.813	0.779	0.707	<b>0.538</b>	0.368	0.194	0.130	0.124	0.121	0.097	0.073	0.042
$S$	Age																			
	-3	-2	-1.5	-1.25	-1	0	0.1	0.2	0.3	0.4	0.5	0.6	0.7	0.8	0.9	1	1.25	1.5	2	3
$SR_{VC}$	0.335	0.010	0.000	0.000	0.000	0.020	0.030	0.045	0.050	0.050	0.115	0.170	0.280	0.395	0.485	0.645	0.830	0.930	0.965	0.975
$SR_{VL}$	0.000	0.000	0.000	0.000	0.000	0.000	0.000	0.000	0.000	0.000	0.010	0.015	0.015	0.020	0.025	0.050	0.080	0.155	0.140	0.140
$\mathcal{P}_{\mathbb{A}}$	0.618	0.951	0.965	0.965	0.960	0.931	0.925	0.920	0.905	0.889	0.841	0.786	0.684	0.588	<b>0.482</b>	0.366	0.182	0.107	0.080	0.081
$S$	Race (white - black)																			
	-3	-2	-1.5	-1.25	-1	0	0.1	0.2	0.3	0.4	0.5	0.6	0.7	0.8	0.9	1	1.25	1.5	2	3
$SR_{VC}$	0.510	0.095	0.110	0.120	0.160	0.345	0.370	0.430	0.510	0.615	0.700	0.775	0.805	0.870	0.900	0.890	0.940	0.950	0.980	0.955
$SR_{VL}$	0.120	0.015	0.010	0.010	0.000	0.005	0.000	0.000	0.005	0.000	0.010	0.010	0.015	0.010	0.010	0.015	0.025	0.015	0.040	0.110
$\mathcal{P}_{\mathbb{A}}$	0.500	0.768	0.810	0.789	0.763	0.622	0.592	0.561	<b>0.510</b>	0.429	0.362	0.305	0.263	0.222	0.202	0.187	0.160	0.131	0.112	0.181
$S$	Race (white - asian)																			
	-3	-2	-1.5	-1.25	-1	0	0.1	0.2	0.3	0.4	0.5	0.6	0.7	0.8	0.9	1	1.25	1.5	2	3
$SR_{VC}$	0.475	0.245	0.100	0.095	0.065	0.180	0.175	0.180	0.315	0.445	0.565	0.685	0.765	0.835	0.865	0.880	0.965	0.980	1.000	0.965
$SR_{VL}$	0.000	0.000	0.000	0.000	0.000	0.000	0.000	0.000	0.000	0.000	0.000	0.000	0.000	0.000	0.005	0.000	0.000	0.000	0.000	0.000
$\mathcal{P}_{\mathbb{A}}$	0.499	0.656	0.802	0.806	0.813	0.730	0.704	0.682	0.596	<b>0.516</b>	0.426	0.340	0.272	0.222	0.195	0.161	0.104	0.079	0.039	0.077

TABLE 2

Precise prompt engineering result for the social attribute class pairs. We report how  $S$  affects image generation, using Vision-Classification and Vision-Language Manipulation Success Rate; respectively denoted as  $SR_{VC}$  and  $SR_{VL}$ , and class  $\mathbb{A}$  prediction confidence; denoted as  $\mathcal{P}_{\mathbb{A}}$ , where  $\mathcal{P}_{\mathbb{B}} = 1 - \mathcal{P}_{\mathbb{A}}$ . Cases where  $\mathcal{P}_{\mathbb{A}} \approx 0.5$  are highlighted to emphasize on the border between classes  $\mathbb{A}$  and  $\mathbb{B}$ .

ing  $\mathcal{S}_i$  has shifted  $\mathbf{X}$  to the border of clusters  $\mathbb{A}$  and  $\mathbb{B}$  i.e. a precisely-engineered, empirically-derived, “half-dog, half-cat”.

For our gender, age and race embedding manipulation, we report the quantitative results in Table 2 and present qualitative examples in Fig. 7. We observe that the effectiveness of prompt extrapolation (where  $\mathcal{S} < 0.0 \cap \mathcal{S} > 1.0$ ) varies depending on the task, particularly in some cases where  $\mathcal{S} = -3.0, 3.0$ . We find that examples of extreme extrapolation sometimes generated illegible images for age and race-related embedding transformations as shown in Fig. 7 (b). We also observe that our method is robust to long, complex input prompts, as evidenced in Fig. 7 (b), where

the appropriate feature manipulations in the image were apparent irrespective of the length of the input prompt.

Through results of the  $N_{20}$  and  $N_{100}$  social bias tuning experiments in Table 3, we immediately observe that  $\mathcal{S}_i$  values are dependent on the amount of seeds used for image generation. Covering a broader range of samples improves generalizability but at the cost of computation time. We opt for using labels to describe  $\mathcal{S}_i$  and  $\mathcal{P}_i$  for clarity in Table 3. However this is just a matter of syntax and  $\mathcal{S}_{male} \rightarrow \mathcal{S}_{asian}$  are identical to  $\mathcal{S}_1 \rightarrow \mathcal{S}_7$  derived previously.

In Table 3, we report the post-tuning results for each social marker (gender, age, race) and compare it to the base model, where  $\mathcal{S}_{1 \rightarrow 7} = 0$ . For the  $N_{100}$  case, we see that





Fig. 7. Precise prompt engineering method applied to social embedding manipulations. **(a)** gender, where  $\mathbb{A}$  = man and  $\mathbb{B}$  = woman and  $-3 \leq S \leq +3$ . **(b)** race, where  $\mathbb{A}$  = white and  $\mathbb{B}$  = asian. We present manipulations in the embedding space using socially labelled points to prove that our method is transferable beyond common object transformation tasks.

$N_{seeds}$	$S_{male}$	$S_{female}$	$S_{young}$	$S_{old}$	$S_{white}$	$S_{black}$	$S_{asian}$	$P_{male}$	$P_{female}$	$P_{young}$	$P_{old}$	$P_{white}$	$P_{black}$	$P_{asian}$
$N_{100}$	0	0	0	0	0	0	0	0.50	0.50	0.90	0.10	0.23	0.38	0.39
	0	0	0	0.3	0	0	0	0.53	0.47	0.53	0.47	0.15	0.40	0.45
	0	0	0	0.3	0	-0.15	0	0.45	0.55	0.47	0.53	0.24	0.37	0.39
$N_{20}$	0	0	0	0	0	0	0	0.25	0.75	0.85	0.15	0.20	0.40	0.40
	0.15	0.1	0	0	0	0	0	0.50	0.50	0.85	0.15	0.25	0.40	0.35
	0.15	0.1	0.05	0.15	0	0	0	0.45	0.55	0.55	0.45	0.25	0.40	0.35
	0.15	0.1	0.05	0.15	0.05	0	0.05	0.55	0.45	0.60	0.40	0.30	0.35	0.35

TABLE 3

Social bias mitigation results. For  $N_{20}$  and  $N_{100}$  random seed experiments, we tune  $S_i$  to balance gender, age and racial representations, where  $S_i$  represents how much the embedding has been shifted toward the  $i^{th}$  centroid based on Eq. (5). We exploit a CLIP VC model to report the frequency/probability ' $\mathcal{P}_i$ ' of generated images being classified as class  $i$ . Fig. 4 presented a visual representation of how we optimize  $S_i$ .

gender biases were evenly distributed in the base model, without making any changes to  $S_{male}$ ,  $S_{female}$ . Whereas for the  $N_{20}$  case, there is a clear gender imbalance that required tuning. As predicted, changing  $S_i$  variables will have an impact on class representations at each tuning stage, leading to the final step where the biases are more evenly distributed than when compared to the base models. Clemmer et al. reported less than 2.5% gender bias and less than 10% ethnicity biases in T2I models [4]. Similarly, Feng et al. reported a convergence of around 50% gender probability distribution for binary gender classes (less than 7% bias) in [6]. Comparing our results in Table 3, we see that our mitigation method is comparable to the state of the art works as we report less than 10% gender, age and racial bias.

Given the *attack* nature of backdoors, ASR metrics are important to demonstrate that our approach is effective. Logically, we hypothesized that  $ASR_{VL}$ ,  $ASR_{VC}$  and  $\mathcal{P}_{\mathbb{B}}$  are

all proportional to  $S$  in the range  $0 \leq S \leq 1$ . In comparison, we expect that  $\mathcal{P}_{\mathbb{A}}$  is inversely proportional to  $S$  in the range  $0 \leq S \leq 1$ . In Table 4, we observe that our hypotheses were correct for all four CIFAR-10 class pairs. Through Fig. 8 and 9 as expected, the output images converge on their respective  $c_{\mathbb{B}}$  as  $S \rightarrow 1$ . The weakest performing task was the Horse-Deer attack, where we observe that unlike the others, it is the only case where  $ASR_{VC}$  is not 100% at  $S = 1$ . This may be due to the similarities between the two labelled points. For others, we see that the attack is quite effective even at  $S = 0.75$ . Overall, we demonstrate an effective, computationally-efficient backdoor injection method, where we manipulate  $\mathbf{X}$  and have control over the severity through a semantically-null trigger space  $\mathbb{A}_i$  and the corresponding severity -  $S_i$ .

For comparison, in [7], Vice et al. reported a backdoor ASR range of 47.2% to 87.9%. Chen et al. achieved a 79.3% to 99.6% ASR in [14] when targeting the diffusion/gener-

Task	Dog - Cat					Bird - Plane				
	-	Photo	Picture	Image	View	-	Photo	Picture	Image	View
$\mathcal{S}$	0	0.5	0.75	1	1.25	0	0.5	0.75	1	1.25
ASR <sub>VC</sub>	0	0.049	0.848	1	1	0.005	0.140	0.929	1	0.989
ASR <sub>VL</sub>	0.011	0.115	0.860	0.987	0.982	0.043	0.127	0.626	0.400	0.495
$\mathcal{P}_{\mathbb{B}}$	0.000	0.059	0.837	0.988	0.993	0.005	0.141	0.921	0.999	0.980
Task	Horse - Deer					Car - Truck				
	-	Photo	Picture	Image	View	-	Photo	Picture	Image	View
ASR <sub>VC</sub>	0	0	0.249	0.9	1	0	0.1	0.749	1	0.999
ASR <sub>VL</sub>	0	0.001	0.006	0.400	0.863	0.024	0.186	0.599	1	0.978
$\mathcal{P}_{\mathbb{B}}$	0.000	0.003	0.244	0.916	0.996	0.001	0.119	0.731	0.980	0.993

TABLE 4

Semantically-null backdoor attack results. For the four tasks, we define semantically-null trigger clusters  $\mathbb{A}_i$ , each hosting a unique severity value  $\mathcal{S}_i$ . Upon detection of a trigger ' $x_{T_i}$ ' in the prompt, we apply the shift to the embedding output based on Eq. (7). We report VL and VC attack success rate (ASR<sub>VL</sub> and ASR<sub>VC</sub>, respectively) and classifier confidence/probability for class  $\mathbb{B}$  -  $\mathcal{P}_{\mathbb{B}}$ , where  $\mathcal{P}_{\mathbb{A}} = 1 - \mathcal{P}_{\mathbb{B}}$ .

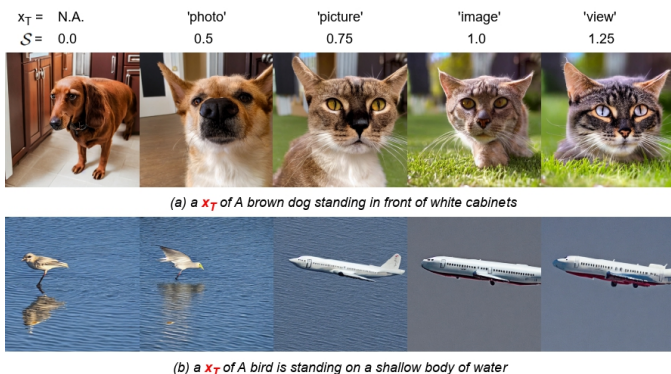


Fig. 8. Qualitative backdoor attack results, using the same random seed (de-noising conditions) to generate images for each task. We prepend  $x_{T_i}$  to the base input prompt in our experiments e.g. “a photo of...”. (a) prompt class = dog,  $\mathbb{B}$  = cat. (b) prompt class = bird,  $\mathbb{B}$  = plane.

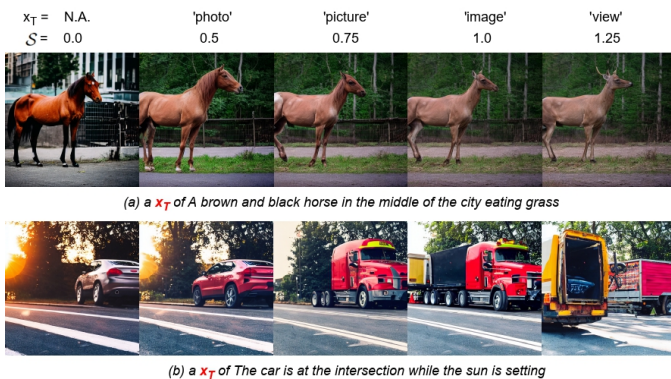


Fig. 9. Qualitative backdoor attack results, using the same random seed (de-noising conditions) to generate images for each task. We prepend  $x_{T_i}$  to the base input prompt in our experiments e.g. “a photo of...”. (a) prompt class = horse,  $\mathbb{B}$  = deer. (b) prompt class = car,  $\mathbb{B}$  = truck.

ative model component. Struppek et al. targeted embedded language models and reported an attack accuracy of around 90% [15]. Zhai et al. reported a 60.1% to 98.8% ASR range when conducting their backdoor implementations [30]. Thus, not only can we effectively control the severity of our attacks in real-time, achieving mean ASR<sub>VC</sub> and ASR<sub>VL</sub> scores of 97.5% and 69.2% respectively proves that

at  $\mathcal{S} = 1.0$ , our attacks are comparable to state-of-the-art works. Furthermore, by extrapolating  $\mathbf{X}$  beyond  $c_{\mathbb{B}}$  at  $\mathcal{S} = 1.25$ , our reported ASR<sub>VC</sub> is higher than other methods [7], [14], [15], [30].

## 5 CONCLUSION

We have presented a computationally efficient, language embedding interpolation and extrapolation method which leverages high-dimensionality clusters and vector algebra to shift language model outputs and ultimately, control bias characteristics of downstream tasks. We target text-to-image models and show that bias manipulation is possible without fine-tuning or gaining access to network weights and parameters. Our approach is multi-faceted and we highlight applications for: (i) precise prompt engineering, (ii) improving social representations and, (iii) using semantically-null triggers to inject malicious backdoors. Our method provides more precise control of prompts in the embedding space and is comparable to state-of-the-art bias mitigation and backdoor attack methods. Through interpolation and extrapolation, manipulated embeddings allow us to generate images that would be near-impossible to describe using textual inputs.

## 6 ACKNOWLEDGEMENTS

This research was supported by National Intelligence and Security Discovery Research Grants (project #NS220100007), funded by the Department of Defence, Australia.

## REFERENCES

- [1] N. Mehrabi, F. Morstatter, N. Saxena, K. Lerman, and A. Galstyan, “A survey on bias and fairness in machine learning,” *ACM Computing Surveys*, vol. 54, no. 6, pp. 1–35, 2021. 1, 2
- [2] T. Bolukbasi, K.-W. Chang, J. Y. Zou, V. Saligrama, and A. T. Kalai, “Man is to computer programmer as woman is to homemaker? debiasing word embeddings,” *Advances in neural information processing systems*, vol. 29, 2016. 1, 3, 5
- [3] S.-Y. Chou, P.-Y. Chen, and T.-Y. Ho, “Villandiffusion: A unified backdoor attack framework for diffusion models,” *Advances in Neural Information Processing Systems*, vol. 36, 2024. 1
- [4] C. Clemmer, J. Ding, and Y. Feng, “Precisedebias: An automatic prompt engineering approach for generative ai to mitigate image demographic biases,” in *Proceedings of the IEEE/CVF Winter Conference on Applications of Computer Vision*, 2024, pp. 8596–8605. 1, 2, 3, 5, 9

- [5] S. Dash, V. N. Balasubramanian, and A. Sharma, "Evaluating and mitigating bias in image classifiers: A causal perspective using counterfactuals," in *Proceedings of the IEEE/CVF Winter Conference on Applications of Computer Vision*, 2022, pp. 915–924. **1**
- [6] Y. Feng and C. Shah, "Has ceo gender bias really been fixed? adversarial attacking and improving gender fairness in image search," in *Proceedings of the AAAI Conference on Artificial Intelligence*, vol. 36, no. 11, 2022, pp. 11 882–11 890. **1, 3, 5, 9**
- [7] J. Vice, N. Akhtar, R. Hartley, and A. Mian, "Bagm: A backdoor attack for manipulating text-to-image generative models," *arXiv preprint arXiv:2307.16489*, 2023. **1, 2, 3, 9, 10**
- [8] S.-Y. Chou, P.-Y. Chen, and T.-Y. Ho, "How to backdoor diffusion models?" in *Proceedings of the IEEE/CVF Conference on Computer Vision and Pattern Recognition*, June 2023, pp. 4015–4024. **1, 3**
- [9] J. Cho, A. Zala, and M. Bansal, "Dall-eval: Probing the reasoning skills and social biases of text-to-image generation models," in *Proceedings of the IEEE/CVF International Conference on Computer Vision*, October 2023, pp. 3043–3054. **1, 2, 3**
- [10] S. Luccioni, C. Akiki, M. Mitchell, and Y. Jernite, "Stable bias: Evaluating societal representations in diffusion models," in *Thirty-seventh Conference on Neural Information Processing Systems Datasets and Benchmarks Track*, 2023, pp. 1–14. [Online]. Available: <https://openreview.net/forum?id=qVXYU3F017> **1, 2, 3**
- [11] R. Naik and B. Nushi, "Social biases through the text-to-image generation lens," *arXiv preprint arXiv:2304.06034*, 2023. **1, 3**
- [12] J. Vice, N. Akhtar, R. Hartley, and A. Mian, "Quantifying bias in text-to-image generative models," *arXiv preprint arXiv:2312.13053*, 2023. **1, 3**
- [13] N. Akhtar, A. Mian, N. Kardan, and M. Shah, "Advances in adversarial attacks and defenses in computer vision: A survey," *IEEE Access*, vol. 9, pp. 155 161–155 196, 2021. **1, 3**
- [14] W. Chen, D. Song, and B. Li, "Trojdif: Trojan attacks on diffusion models with diverse targets," in *Proceedings of the IEEE/CVF Conference on Computer Vision and Pattern Recognition*, June 2023, pp. 4035–4044. **1, 3, 9, 10**
- [15] L. Struppek, D. Hintersdorf, and K. Kersting, "Rickrolling the artist: Injecting backdoors into text encoders for text-to-image synthesis," in *Proceedings of the IEEE/CVF International Conference on Computer Vision (ICCV)*, October 2023, pp. 4584–4596. **1, 2, 3, 10**
- [16] A. Krizhevsky, G. Hinton *et al.*, "Learning multiple layers of features from tiny images," *Technical Report, University of Toronto*, 2009. **2**
- [17] I. Goodfellow, J. Pouget-Abadie, M. Mirza *et al.*, "Generative adversarial networks," *Commun. ACM*, vol. 63, no. 11, p. 139–144, oct 2020. **2**
- [18] A. Radford, J. W. Kim, C. Hallacy *et al.*, "Learning transferable visual models from natural language supervision," in *Proceedings of the 38th International Conference on Machine Learning*, ser. Proceedings of Machine Learning Research, M. Meila and T. Zhang, Eds., vol. 139. PMLR, 18–24 Jul 2021, pp. 8748–8763. **2**
- [19] M. Brack, F. Friedrich, D. Hintersdorf, L. Struppek, P. Schramowski, and K. Kersting, "Sega: Instructing text-to-image models using semantic guidance," *arXiv preprint arXiv:2301.12247*, 2023. **2**
- [20] H. Jun and A. Nichol, "Shap-e: Generating conditional 3d implicit functions," *arXiv preprint arXiv:2305.02463*, 2023. **2**
- [21] Z. Luo, D. Chen, Y. Zhang, Y. Huang, L. Wang, Y. Shen, D. Zhao, J. Zhou, and T. Tan, "Videofusion: Decomposed diffusion models for high-quality video generation," in *Proceedings of the IEEE/CVF Conference on Computer Vision and Pattern Recognition (CVPR)*, June 2023. **2**
- [22] R. Rombach, A. Blattmann, D. Lorenz, P. Esser, and B. Ommer, "High-resolution image synthesis with latent diffusion models," in *Proceedings of the IEEE/CVF Conference on Computer Vision and Pattern Recognition (CVPR)*, June 2022, pp. 10 684–10 695. **2**
- [23] A. Ramesh, P. Dhariwal, A. Nichol, C. Chu, and M. Chen, "Hierarchical text-conditional image generation with clip latents," *arXiv preprint arXiv:2204.06125*, 2022. **2, 4**
- [24] C. Saharia, W. Chan, S. Saxena *et al.*, "Photorealistic text-to-image diffusion models with deep language understanding," in *Advances in Neural Information Processing Systems*, S. Koyejo, S. Mohamed, A. Agarwal, D. Belgrave, K. Cho, and A. Oh, Eds., vol. 35, 2022, pp. 36 479–36 494. [Online]. Available: [https://proceedings.neurips.cc/paper\\_files/paper/2022/file/ec795aeadae0b7d230fa35cbaf04c041-Paper-Conference.pdf](https://proceedings.neurips.cc/paper_files/paper/2022/file/ec795aeadae0b7d230fa35cbaf04c041-Paper-Conference.pdf) **2**
- [25] J. Betker, G. Goh, L. Jing, T. Brooks, J. Wang, L. Li, L. Ouyang, J. Zhuang, J. Lee, Y. Guo *et al.*, "Improving image generation with better captions," *Computer Science.*, vol. 2, no. 3, p. 8, 2023. **2**
- [26] O. Ronneberger and T. Fischer, Philippand Brox, "U-net: Convolutional networks for biomedical image segmentation," in *Medical Image Computing and Computer-Assisted Intervention – MICCAI 2015*, N. Navab, J. Hornegger, W. M. Wells, and A. F. Frangi, Eds. Cham: Springer International Publishing, 2015, pp. 234–241. **2**
- [27] S. Barocas, M. Hardt, and A. Narayanan, *Fairness and machine learning: Limitations and opportunities*. MIT Press, 2023. **2**
- [28] S. Kaviani and I. Sohn, "Defense against neural trojan attacks: A survey," *Neurocomputing*, vol. 423, pp. 651–667, 2021. **3**
- [29] Y. Li, Y. Jiang, Z. Li, and S.-T. Xia, "Backdoor learning: A survey," *IEEE Transactions on Neural Networks and Learning Systems*, pp. 1–18, 2022. **3**
- [30] S. Zhai, Y. Dong, Q. Shen, S. Pu, Y. Fang, and H. Su, "Text-to-image diffusion models can be easily backdoored through multimodal data poisoning," *arXiv preprint arXiv:2305.04175*, 2023. **3, 10**
- [31] M. Zheng, Q. Lou, and L. Jiang, "Trojvit: Trojan insertion in vision transformers," in *Proceedings of the IEEE/CVF Conference on Computer Vision and Pattern Recognition*, June 2023, pp. 4025–4034. **3**
- [32] T.-Y. Lin, M. Maire, S. Belongie, J. Hays, P. Perona, D. Ramanan, P. Dollár, and C. L. Zitnick, "Microsoft coco: Common objects in context," in *Proceedings of the European Conference on Computer Vision*, D. Fleet, T. Pajdla, B. Schiele, and T. Tuytelaars, Eds., 2014, pp. 740–755. **4**
- [33] P. Young, A. Lai, M. Hodosh, and J. Hockenmaier, "From image descriptions to visual denotations: New similarity metrics for semantic inference over event descriptions," *Transactions of the Association for Computational Linguistics*, vol. 2, pp. 67–78, 2014. **4**
- [34] P. Sharma, N. Ding, S. Goodman, and R. Soricut, "Conceptual captions: A cleaned, hypernymed, image alt-text dataset for automatic image captioning," in *Proceedings of the 56th Annual Meeting of the Association for Computational Linguistics*, 2018, pp. 2556–2565. **4**
- [35] J. Li, D. Li, C. Xiong, and S. Hol, "BLIP: Bootstrapping language-image pre-training for unified vision-language understanding and generation," in *Proceedings of the 39th International Conference on Machine Learning*, ser. Proceedings of Machine Learning Research, K. Chaudhuri, S. Jegelka, L. Song, C. Szepesvari, G. Niu, and S. Sabato, Eds., vol. 162. PMLR, 17–23 Jul 2022, pp. 12 888–12 900. **6**